TheRate: Program for *Ab Initio* Direct Dynamics Calculations of Thermal and Vibrational-State-Selected Rate Constants

WENDELL T. DUNCAN, ROBERT L. BELL, and THANH N. TRUONG
Department of Chemistry, University of Utah, Salt Lake City, Utah 84112

Received 5 August 1997; accepted 10 February 1998

ABSTRACT: We introduce TheRate (THEoretical RATEs), a complete application program with a graphical user interface (GUI) for calculating rate constants from first principles. It is based on canonical variational transition-state theory (CVT) augmented by multidimensional semiclassical zero and small curvature tunneling approximations. Conventional transition-state theory (TST) with one-dimensional Wigner or Eckart tunneling corrections is also available. Potential energy information needed for the rate calculations are obtained from *ab initio* molecular orbital and/or density functional electronic structure theory. Vibrational-state-selected rate constants may be calculated using a diabetic model. TheRate also introduces several technical advancements, namely the focusing technique and energy interpolation procedure. The focusing technique minimizes the number of Hessian calculations required by distributing more Hessian grid points in regions that are critical to the CVT and tunneling calculations and fewer Hessian grid points elsewhere. The energy interpolation procedure allows the use of a computationally less demanding electronic structure theory such as DFT to calculate the Hessians and geometries, while the energetics can be improved by performing a small number of single-point energy calculations along the MEP at a more accurate level of theory. The $CH_4 + H \leftrightarrow CH_3 + H_2$ reaction is used as a model to demonstrate usage of the program, and the convergence of the rate constants with respect to the number of electronic structure calculations. © 1998 John Wiley & Sons, Inc. J Comput Chem 19: 1039–1052, 1998

Keywords: kinetics; thermal rate constants; direct dynamics; variational transition-state theory

Correspondence to: T. N. Truong; e-mail: Truong@chemistry.utah.edu

CCC 0192-8651 / 98 / 091039-14

Introduction

The fields of computational fluid dynamics, process simulation and design, combustion, and atmospheric chemistry are just a few of the areas that need accurate rate constants of the underlying elementary chemical reactions.[1–3] Predicting rate constants is in fact a major goal of computational chemistry.[4] The TheRate (THEoretical RATEs) program seeks to bring together many of the recent advances in computational chemistry methods in a user-friendly environment to calculate elementary reaction rate constants from first principles, and seeks to bridge the gap between chemistry and chemical engineering.

Calculations of rate constants require a delicate balance between the accuracy of the dynamical theory and the efficiency in obtaining accurate potential energy information. In the extreme of rigorous dynamical treatment, accurate quantum dynamics calculations yield detailed state-to-state reactive cross-sections or rate constants with full consideration of quantum effects.[5–9] However, such calculations are currently limited to four-atom reacting systems with the use of global analytical potential energy functions. In the other extreme, transition-state theory (TST) has been practical for a wide range of chemical processes due to its simplicity. The basic model only requires potential energy information at the reactant(s) and transition state, because it treats many dynamical effects only approximately. The major advantage of TST is that such limited potential energy information may be obtained from accurate electronic structure calculations without the need of an analytical potential energy function. Variational effects and/or tunneling are important in many reactions, and for these systems more accurate dynamical treatments are desirable. For instance, variational transition state theory (CVT)[10,11] provides a well-established methodology to bridge this gap. In this case, more information on the potential energy surface is needed. Conventionally, the additional information is obtained by first constructing an analytical potential function which is fitted to results from accurate electronic structure calculations and available experimental data.[12–14] This becomes an impossible task as the size of the reacting system increases, because: (i) the number of energy points required grows geometrically with the number of internal coordinates; (ii) potential functional forms are arbitrary; and (iii) fitting procedures do not guarantee convergence and correct global topology.[12] The direct dynamics approach offers a viable alternative for studying the kinetics and dynamics of complex systems. In the direct dynamics approach, all required energies, forces, and geometries needed to evaluate dynamical properties are obtained directly from electronic structure calculations rather than from empirical analytical force fields.[15–21]

The direct dynamics approach, however, is limited by the computational demand of electronic structure calculations. For thermal rates, reaction path Hamiltonian methods[22–25] such as the canonical variational transition-state theory (CVT) are particularly attractive due to the limited amount of potential energy and Hessian information that is required.[26] Direct dynamics with CVT thus offers an efficient and cost-effective methodology. Furthermore, several theoretical reviews[27,28] have indicated that CVT plus multidimensional semiclassical tunneling approximations yield accurate rate constants not only for gas-phase reactions but also for chemisorption and diffusion on metals. To fully converge thermal rate constants, however, existing methodologies require a large number of Hessian points along the reaction coordinate. Computationally, it is expensive if these Hessians are to be calculated at an accurate level of *ab initio* molecular orbital theory.

Several approaches have been proposed to reduce this computational demand. One approach is to estimate rate constants and tunneling contributions by using the Interpolated CVT when available accurate *ab initio* electronic structure information is very limited.[29] Another is to carry out CVT calculations with multidimensional semiclassical tunneling approximations using a semiempirical molecular orbital Hamiltonian at the neglect-of-diatomic-differential-overlap (NDDO) level as a fitting function in which NDDO parameters have been readjusted to represent accurately activation energy for specific reactions.[30,31] Both of these approaches have been applied successfully to various gas-phase chemical reactions.[17,32–44] However, many difficulties persist. In particular, in the former interpolated CVT approach, it is difficult to correlate vibrational modes at the transition-state region to reactant and product asymptotes due to mode crossings that occur in most polyatomic systems. In the latter, it may prove to be difficult to adjust the original NDDO parameters to describe accurately the transition-state region if the original NDDO potential energy surface differs signifi-

cantly from the reference accurate *ab initio* surface. Furthermore, even if the parameters are adjusted to reproduce the barrier height and force constants at the transition state,[31] there is no guarantee that the reaction path curvature and coupling between vibrational modes and reaction coordinate are correct. These factors directly affect the computed tunneling probability and product-state distributions.[45] Recent development in combining both approaches into what is known as dual-level dynamics[16,19,46] has shown some promise.

Our own efforts, however, have been to develop methodologies for reducing computational demand while carrying out CVT calculations with multidimensional semiclassical tunneling corrections directly from a sufficiently accurate level of *ab initio* molecular orbital (MO) and/or density functional theory (DFT) without invoking any potential fitting procedure.[17,18,37,47–51] We attack this problem from three separate fronts. First, we propose the use of a nonlocal DFT functional[52] for determining geometries, gradients, and Hessians along the reaction coordinates. In particular, the hybrid Becke half-and-half exchange[53] with Lee–Yang–Parr[54] correlation functionals (BHH-LYP), as implemented in the Gaussian program,[55] has been found to give quite accurate geometries and frequencies along the reaction path with a lower computational cost than correlated levels of *ab initio* MO theory and yet often yields comparable accuracy, particularly for large systems. We have discussed the accuracy of the BHH-LYP method at length in previous studies.[18,47,56] Note that development of DFT functionals is currency a very active research area. More accurate DFT functionals, as they become available, may be used for calculating reaction path information. Second, we have developed a focusing technique to minimize the number of calculated Hessians along the reaction coordinate. Third, we have developed an interpolation approach for improving the accuracy of the energetics information along the reaction coordinate from a minimal number of additional single-point calculations at a higher level of theory with a larger basis set. We will discuss the latter two efforts in this study.

In addition to being an advanced research tool, this program is also envisioned to be a useful teaching tool for graduate-level kinetics courses. For this purpose, a brief synopsis of the underlying dynamical theories, namely transition-state theory, canonical variational transition-state theory, and various semiclassical tunneling approximations, is provided. The accuracy and convergence of the focusing technique and energy interpolation procedure are then described. The $CH_4 + H \leftrightarrow CH_3 + H_2$ reaction is used to analyze these technical advances, and to demonstrate the program usage.

Transition-State Theory

Transition state theory,[57–62] or activated complex theory, is a well-developed formalism for obtaining thermal rate constants by mixing the important features of the potential energy surface with a statistical representation of the dynamics.

In addition to the Born–Oppenheimer approximation, TST is based on three assumptions: First, classically, there exists a surface in phase space that divides it into a reactant region and a product region. It is assumed that this dividing surface is located at the transition state which is defined as the maximum value on the minimum energy path (MEP) of the potential energy surface that connects the reactant(s) and product(s). Any trajectory passing through the dividing surface (or bottleneck) from the reactant side is assumed to form products eventually. This is often referred to as the nonrecrossing rule. Second, the reactant equilibrium is assumed to maintain a Boltzmann energy distribution. Finally, activated complexes are assumed to have Boltzmann energy distributions corresponding to the temperature of the reacting system. These activated complexes are defined as supermolecules having configurations located in the vicinity of the transition state.

The thermal rate constant, $k(T)$, for a bimolecular reaction $A + B \rightarrow C + D$ is given by

$$k = \sigma \frac{k_b T}{h} \frac{q'_{\ddagger}}{N_a q_A q_B} \exp(-\beta \Delta V^{\ddagger}) \qquad (1)$$

where k_b is Boltzmann's constant, T is the temperature, N_a is Avogadro's number, h is Planck's constant, and β is $1/k_b T$. $\Delta V^{\ddagger}$ is the classical barrier height; that is, the potential energy difference between the reactants and transition state. q_A and q_B denote the respective total partition functions[57,58,63] of the reactants with the translational partition functions expressed in per unit volume. The partition function of the activated complex is $q'_{\ddagger}$ and does not include translational motion along the reaction coordinate because this is treated separately. The reaction symmetry number, σ, represents the number of indistinguishable ways the

reactants may approach the activated complex region. We will discuss forward and reverse reaction symmetry numbers in more detail later.

Variational Transition-State Theory

Canonical variational transition-state theory (CVT) is an extension of transition state theory.[64–67] It minimizes the recrossing effects and provides a framework for a more accurate description of quantum tunneling effects to be considered.

CVT minimizes the recrossing effects by effectively moving the dividing surface along the MEP between the reactants and products so as to minimize the rate. The reaction coordinate, s, is defined as the distance along the MEP calculated in mass-weighted Cartesian coordinates with the origin located at the saddle point and is positive on the product side and negative on the reactant side. For a canonical ensemble at a given temperature T, the canonical variational theory (CVT) rate constant for a bimolecular reaction is given by:

$$k^{CVT}(T) = \min_{s} k^{GT}(T, s) \tag{2}$$

where:

$$k^{GT}(T, s) = \sigma \frac{kT}{h} \frac{q^{GT}(T, s)}{N_a q_A q_B} \exp(-\beta V_{MEP}(s)) \tag{3}$$

In these equations, $k^{GT}(T, s)$ is the generalized transition-state theory rate constant where the dividing surface is perpendicular to the MEP and intersecting it at s. $q^{GT}(T, s)$ is the partition function of the generalized transition state at s with the motion along the reaction coordinate removed. $V_{MEP}(s)$ is the classical potential energy (the Born–Oppenheimer potential energy) along the MEP with the zero of energy at the reactants. Note that if the generalized transition state is located at the saddle point ($s = 0$), eq. (3) reduces to that of conventional TST.

CVT yields hybrid rate constants that treat motion along the reaction coordinate classically. Quantum effects in this degree of freedom are included by multiplying the CVT rate constant by a ground-state transmission coefficient $\kappa(T)$. Thus, the final CVT rate constant is given by:

$$k(T) = \kappa(T) k^{CVT}(T) \tag{4}$$

Forward and Reverse Reaction Symmetries

The reaction symmetry number,[62, 68–70] which appeared in the rate expression, is the ratio of the rotational symmetry numbers and is also known as the statistical factor. It describes the number of symmetry equivalent reaction paths. For bimolecular reactions, the forward reaction symmetry number is computed using the following formula:

$$\sigma_f = \frac{\mathrm{NSYM}(\mathit{Reactant}\ 1) * \mathrm{NYSM}(\mathit{Reactant}\ 2)}{\mathrm{NSYM}(GTS)} \tag{5}$$

where NSYM is the symmetry number associated with the point group to which the considered molecular configuration belongs. Similarly, the reverse symmetry number is given by:

$$\sigma_r = \frac{\mathrm{NSYM}(\mathit{Product}\ 1) * \mathrm{NSYM}(\mathit{Product}\ 2)}{\mathrm{NSYM}(GTS)} \tag{6}$$

For optically active molecules there is an extra correction because each optically active isomer represents distinct, but energetically equivalent, states. Each optically active configuration should be given an extra factor of 1/2.[68]

We use the $CH_3 + HCl \leftrightarrow CH_4 + Cl$ reaction as an illustrative example. From Table I[71] we find that the CH_4Cl complex belongs to the C_{3v} point group with NSYM = 3. The CH_3 reactant belongs to the D_{3h} point group with NSYM = 6. The HCl reactant belongs to the $C_{\infty v}$ point group with

TABLE I.
Symmetry Number of Various Point Groups.[71]

Point group	NSYM	Point group	NSYM
C_1, C_i, C_s	1	Atom	1
C_2, C_{2v}, C_{2h}	2	D_2, D_{2d}, D_{2h}	4
C_3, C_{3v}, C_{3h}	3	D_3, D_{3d}, D_{3h}	6
C_4, C_{4v}, C_{4h}	4	D_4, D_{4d}, D_{4h}	8
C_5, C_{5v}, C_{5h}	5	D_5, D_{5d}, D_{5h}	10
C_6, C_{6v}, C_{6h}	6	D_6, D_{6d}, D_{6h}	12
C_7	7	C_8	8
D_{8h}	16	S_4	2
S_6	3	S_8	4
$C_{\infty v}$	1	$D_{\infty h}$	2
T, T_d, T_h	12	O, O_h	24
I_h	60		

NSYM = 1. The Cl product atom belongs to the spherical orthogonal point group with NSYM = 1. The CH_4 product belongs to the T_d point group with NSYM = 12. The forward reaction symmetry is then:

$$\sigma_f = \frac{6*1}{3} = 2 \tag{7}$$

and the reverse reaction symmetry is:

$$\sigma_r = \frac{12*1}{3} = 4 \tag{8}$$

For some reactions the transition state belongs to a higher symmetry point group than other points along the MEP. Consider for example the $S_{N2}Cl^- + CH_3Cl$ reaction—the transition state has D_{3h} symmetry, whereas points along the MEP only have C_{3v} symmetry. In this case, the lower symmetry point group should be used, even in TST calculations, because the activated complexes in general have lower symmetry with the transition state representing a special case.

Tunneling Methods

The current TheRate version includes four different semiclassical methods for calculating the transmission coefficients, $\kappa(T)$; namely the one-dimensional Wigner and Eckart methods and, the multidimensional zero-curvature and centrifugal-dominant small-curvature methods.[27,34,64,72] For convenience, we label them as W, ECK, ZCT, and SCT, respectively.

For TST rates, the Wigner and Eckart transmission probabilities are used. For CVT rates, the ZCT and SCT transmission probabilities are utilized. The Eckart method is a special case of the ZCT calculation where the potential energy for tunneling is fitted by an Eckart function. Also, the ZCT method is limiting case of the SCT method. These methods are described in detail in what follows.

WIGNER TUNNELING CORRECTION

The Wigner correction for tunneling assumes a parabolic potential for the nuclear motion near the transition state[64]:

$$V(x) = V_o - \frac{1}{2} m \omega^{\ddagger} x^2 \tag{9}$$

where V_o is the energy at the top of the barrier, and $\omega^{\ddagger}$ is the imaginary frequency of the transition state. The Wigner tunneling correction, $\kappa(T)$ then is given by:

$$\kappa(T) = 1 + \frac{1}{24}[\hbar \omega^{\ddagger} \beta]^2 \tag{10}$$

where β is $1/k_bT$. Thus, the Wigner correction only requires the imaginary frequency at the transition state.

SMALL-CURVATURE TUNNELING

First, we approximate the effective potential for tunneling to be:

$$V_d(s) = V_{MEP}(s) + \sum_{i=1}^{3N-7} \left(\frac{1}{2} + m_i \right) \hbar \omega_i(s) \tag{11}$$

where m_i is the vibrational state of mode i orthogonal to the MEP. If all vibrational modes are in their ground state, $V_d(s)$ is equivalent to the vibrationally adiabatic ground state potential curve $V_a^G(s)$, which is used in calculations of tunneling contributions to thermal rate constants. The transmission coefficient, $\kappa(T)$, is then approximated as the ratio of the thermally averaged multidimensional semiclassical transmission probability, $P^G(E)$, to the thermally averaged classical transmission probability for scattering by the effective potential, $V_d(s)$. If we denote the CVT transition state at temperature T as $s_*^{CVT}(T)$, then the quasiclassical threshold energy, $V_d\{s_*^{CVT}(T)\}$, can be denoted as $E_*(T)$. The equation for $\kappa(T)$ then becomes[67]:

$$\kappa(T) = \frac{\int_0^{\infty} P(E) e^{-E/k_bT}\, dE}{\int_{E_*(T)}^{\infty} e^{-E/k_bT}\, dE} \tag{12}$$

Notice that the integral in the numerator of eq. (12) involves E above $E_*(T)$, as well as tunneling energies below this. Thus, the semiclassical transmission probability, $P(E)$, accounts for both nonclassical reflection at energies above the quasiclassical threshold and nonclassical transmission (i.e., tunneling, at energies below that threshold). Because of the Boltzmann factor in eq. (12), tunneling is by far the more important of these two quantum effects.

The centrifugal-dominant small-curvature semiclassical approximation[73] (SCT) is a generalization of the Marcus–Coltrin[74] approximation in which

the tunneling path is distorted from the MEP out to a concave-side vibrational turning point in the direction of the internal centrifugal force. Instead of explicitly defining this tunneling path, the centrifugal effect is included by replacing the reduced mass by an effective reduced mass, $\mu_{eff}(s)$, which is used to evaluate the imaginary action integral and thereby tunneling probabilities. Note that, in the mass-weighted Cartesian coordinate system, the reduced mass, μ, is set equal to 1 amu. The transmission probability at energy E is:

$$P(E) = \frac{1}{\{1 + e^{2\theta(E)}\}} \tag{13}$$

where $\theta(E)$ is the imaginary action integral evaluated along the tunneling path:

$$\theta(E) = \frac{2\pi}{h}\int_{s_l}^{s_r}\sqrt{2\mu_{eff}(s)|E - V_d(s)|}\, ds \tag{14}$$

The integration limits, s_l and s_r, are the reaction-coordinate classical turning points defined by:

$$V_d[s_l(E)] = V_d[s_r(E)] = E \tag{15}$$

Note that the ZCT results can be obtained by setting $\mu_{eff}(s)$ equal to μ in eq. (14). The effect of the reaction-path curvature included in the effective reduced mass $\mu_{eff}(s)$ is explained in what follows.

The small-curvature tunneling amplitude corresponds approximately to an implicit tunneling path that follows the line of concave-side vibrational turning point at a distance, $\bar{t}(s)$, from the MEP in the direction of the reaction-path curvature vector. Let the distance along the small-curvature tunneling path be ξ and the curvature at s be $\kappa(s)$; then, it can be shown by analytical geometry that:

$$d\xi = \sqrt{\left\{[1 - \bar{a}(s)]^2 + \left[\frac{d\bar{t}(s)}{ds}\right]^2\right\}}\, ds \tag{16}$$

where:

$$\bar{a}(s) = |\kappa(s)\bar{t}(s)| \tag{17}$$

The imaginary action integral along the small-curvature tunneling path is defined as:

$$\theta(E) = \frac{2\pi}{h}\int\sqrt{2\mu|E - V_a[s(\xi)]|}\, d\xi \tag{18}$$

By comparing eqs. (14) and (18), the effective reduced mass is given by:

$$\mu_{eff}(s) = \mu\left\{[1 - \bar{a}(s)]^2 + \left[\frac{d\bar{t}(s)}{ds}\right]^2\right\} \tag{19}$$

However, to make the method generally applicable, even when $\bar{t}(s)$ is greater than or equal to the radius of cunature of the reaction path, we include only the leading terms of eq. (19), but not singularities by the approximated form:

$$\mu_{eff}(s) = \mu \times \min\left\{\begin{matrix}\exp\{-2\bar{a}(s) - [\bar{a}(s)]^2 + (d\bar{t}/ds)^2\} \\ 1\end{matrix}\right. \tag{20}$$

The magnitude of the reaction-path curvature, $\kappa(s)$, is given by[75]:

$$\kappa(s) = \left\{\sum_{i=1}^{F-1}[\kappa_i(s)]^2\right\}^{1/2} \tag{21}$$

where the summation is over all generalized normal modes ($i = 1, 2, 3, \ldots, F - 1$), and $\kappa_i(s)$ is the reaction-path curvature component of mode i given by:

$$\kappa_i(s) = -\mathbf{L}_i^T\mathbf{F}\frac{\nabla\mathbf{V}}{|\nabla\mathbf{V}|^2} \tag{22}$$

where $\mathbf{L}_i^T$ is the transpose of the generalized normal mode eigenvector of mode i, $\mathbf{F}$ is the force constant matrix (Hessian matrix), and $\nabla\mathbf{V}$ is the gradient. Finally, within the harmonic approximation, $\bar{t}(s)$ is given by[49]:

$$\bar{t}(s) = \left(\frac{\kappa\hbar}{\mu}\right)^{1/2}\left\{\frac{\sum_i^{F-1}[\kappa_i(s)]^2\omega_i^2(s)}{(1 + 2m_i)}\right\}^{-1/4} \tag{23}$$

where ω_i is the generalized vibrational frequency of mode i in state m_i.

ECKART TUNNELING CORRECTION

This methodology[34] requires no *ab initio* calculations at points other than reactants, products, and saddle point. It uses the zero-curvature methodology developed in the previous section. $\kappa(T)$ is evaluated with an approximated adiabatic

ground-state potential energy curve, V_a^G based on an Eckart function.

First, we approximate the classical potential energy, $V_{MEP}(s)$ by an Eckart function whose parameters are calculated from the classical potential energies at the reactants (R), saddle point (‡), and products (P), and from the imaginary frequency. This fit yields the range parameter:

$$\alpha^2 = -\frac{\mu(\omega^{\ddagger})^2 B}{2V^{\ddagger}(V^{\ddagger} - A)} \tag{24}$$

where $V^{\ddagger}$ is the classical barrier height, $\omega^{\ddagger}$ is the imaginary frequency, μ is the reduced mass,

$$A = V_{MEP}(s = +\infty), \quad \text{and}$$
$$B = (2V^{\ddagger} - A) + 2\sqrt{V^{\ddagger}(V^{\ddagger} - A)}\,.$$

V_a^G is then approximated by another Eckart function, which is assumed to have the same range parameter (α) and location of the maximum ($s = 0$) as the classical $V_{MEP}(s)$ approximation. This Eckart function goes through the zero-point-corrected energies at the reactants, saddle point, and products. This yields:

$$V_a^G(s) = \frac{ay}{1 + y} + \frac{by}{(1 + y)^2} + c \tag{25}$$

where:

$$y = e^{\alpha(s - s_o)} \tag{26}$$

$$a = V_a^G(s = +\infty) - V_a^G(s = -\infty) \tag{27}$$

$$b = (2\,\Delta V_a^{\ddagger G} - a) + 2\sqrt{\Delta V_a^{\ddagger G}(\Delta V_a^{\ddagger G} - a)} \tag{28}$$

$$c = \varepsilon_{int}^G(s = -\infty) \tag{29}$$

and:

$$s_o = -\frac{1}{\alpha}\ln\left(\frac{a + b}{b - a}\right) \tag{30}$$

Here, $\Delta V_a^{\ddagger G}$ is the zero-point energy corrected barrier at the saddle point, relative to reactants, and $\varepsilon_{int}^G(s = -\infty)$ is the sum of the zero-point energies of the two reactants.

For most reactions, the zero-point energy correction often lowers the barrier. In this case, the range parameter, α, for the V_a^G curve should be larger; that is, the width of the V_a^G curve is wider than that of the V_{MEP} curve. Thus, the approximation of using the same α for V_{MEP} and V_a^G curves often overestimates the tunneling probability. We have found that, in many cases, this error is compensated for by the ''corner cutting'' effects (see SCT methodology) that are not included in this methodology.

Vibrational-State-Selected Reactions

TheRate provides an option to calculate rate constants with specific initial reactant vibrational states.[47,76] To do this, the vibrational modes along the reaction coordinate are first correlated as discussed later (see ''Technical Considerations'' in Appendix A). A statistical vibrationally diabetic model,[76,77] which assumes that the vibrational modes preserve their characteristic motions as the complex moves along the reaction coordinate, is then used. In the statistical–diabatic model the expression for the vibrational-state-selected rate constants differ from the statistical form for the thermal rate in the vibrational partition function for the selected mode and in the potential energy curve used for the tunneling calculations [see eq. (11)]. The vibrational partition of the mode i in the selected state m is given by:

$$q_i(m, T) = e^{-(1/2 + m)\hbar\omega_i/k_bT} \tag{31}$$

This partition function replaces the thermal distribution partition function for the selected vibrational mode.

The statistical–diabatic model is expected to provide only semiquantatitive state-selected rate constants because vibrational–vibrational and vibrational–rotational couplings were not included. Nevertheless, it gives useful insight into vibrational-state specificity of gas-phase polyatomic reactions.

Focusing Technique

The main goal of the focusing technique is to minimize the computational cost of calculating Hessians along the MEP while maintaining a reasonable level of accuracy in the calculated rate constants. This is done by focusing the computational efforts to regions of the MEP that are most sensitive to the rate calculations. For reactions with reasonable barriers, CVT rate constants are sensitive to regions near the transition state, whereas ZCT and SCT tunneling contributions show strong dependencies not only on the barrier height, but also on the barrier width and the reaction path curvature. It is important to point out that regions

with large reaction path curvature are often not in the vicinity of the transition state. It is an empirical fact borne out from our many applications using the reaction path Hamiltonian[22] approach that such regions coincide with those having large curvature in the geometrical parameters as functions of the reaction coordinate.

Based on this observation, we have designed a weighting function based on the sum of the normalized curvatures of the bond distances, angles, and dihedral angles as functions of the reaction coordinate and the potential curve, each with different relative weightings. Thus, this function weights the importance of different regions along the MEP so as to obtain both accurate CVT rate constants and SCT tunneling contributions. We found that weight factors of 1.0 for bond distances, 0.5 for angles and dihedral angle, and 2.0 for the potential energy curve work well for many tested reactions. Users have the option to change these factors in TheRate to suit different types of reactions. For instance bond-breaking processes would weight bond distances more than angles, but the reverse is more appropriate for studying internal rotation processes. The curvatures of geometrical parameters as functions of the reaction coordinate are determined from piecewise quadratic fits to intervals of eight data points along the MEP using single-value decomposition. This weighting function is used to distribute a given number of points along the MEP for further Hessian calculations.

Energy Interpolation Technique

The accuracy of the potential energy along the MEP is critical for quantitative prediction of rate constants. However, it is often true that the Hessian and geometrical information along the MEP converges with respect to the level of theory and basis set faster than the energy. It is therefore desirable to find the geometries and Hessians at a lower level of theory and then improve the energetic information by performing single-point energy calculations at a higher level of theory and/or a larger basis set. Because these energy calculations are often computationally expensive, we have developed an interpolation technique that only requires a small subset of the Hessian calculation points for more accurate single-point energy calculations.

Typically, the energy points are interpolated directly from the single-point calculations. However, in our interpolation procedure, we instead interpolate the energy correction to the potential energy curve already obtained at the lower level of theory. The energy difference between results from the two levels of theory is calculated at selected points of the Hessian grid. This correction term is cubic spline interpolated, and then added back into the potential energy result from the lower level of theory. As discussed in what follows, by using this technique, very few single-point energy calculations are needed.

An automated method is provided in the TheRate software for selecting a user-given number of points along the MEP for single-point energy calculations. Six to ten points are typically sufficient.

Note that the location of the maximum on the more accurate potential curve is often shifted from the saddle point calculated from the lower level. The origin of the reaction coordinate, s, is then shifted accordingly in CVT calculations, so proper variational effects are calculated.

Model Reaction

To illustrate the use and effectiveness of these techniques, we have performed calculations on the $CH_4 + H \leftrightarrow CH_3 + H_2$ reaction using different Hessian and energy grids. Because the motivating factor of this work is to elucidate the technique, instead of predicting accurate thermal rate constants, a low level of electronic structure theory suffices. We refer to our previous work for accurate rate calculations of this reaction.[17,47] Here we used the STO-3G basis set in conjunction with unrestricted Hartree–Fock (UHF) theory to calculate the MEP information. The MEP was calculated in mass-weighted Cartesian coordinates using a step size of 0.01 $amu^{1/2}$bohr for 100 points on each side of the transition state using the Gonzalez–Schlegel method.[78,79]

FOCUSING TECHNIQUE ANALYSIS

We used Hessian grids of 7, 10, 12, 15, 20, 25, 30, 40, and 50 points to test our focusing technique. Figure 1 shows how various geometrical parameters change along the reaction coordinate from the reactants to the products. Figure 2 shows a second derivative analysis of the geometries and placement of the Hessian grids with various totals. There is some small noise in the graph near the transition state due to inaccuracies in the MEP in

this region. This is due to the linear first step off the transition state that often causes some small oscillatory motion for several subsequent steps along the MEP. Also shown is a normalized energy graph and the sum of the two energy and geometry weightings. As described in the Theory section, the sum is used to bin weight distribute the Hessian grid points. Figure 2 also shows the points selected for further Hessian calculations with differing selected numbers of total Hessians.

Figure 3 shows the change in frequencies calculated in Cartesian coordinates of the reaction path Hamiltonian versus the reaction coordinate. The four graphs are constructed using 7, 15, 25, and 50 total Hessian calculations. Fifteen points are sufficient to show all major features of the reaction, whereas 25 points are needed to provide smooth curves from reactants to products. Typically, between 20 and 30 frequency data points along an MEP are sufficient to obtain smooth correlated frequencies.

Figure 4 shows the curvature component of B_{mf} coupling as a function of the reaction coordinate using 50 Hessian calculations. The SCT "corner cutting" effects are large in regions with significant reaction path curvature. A comparison of the B_{mf} curves with the weighting curves show that our weighting scheme has correctly identified the areas where the curvature components are large.

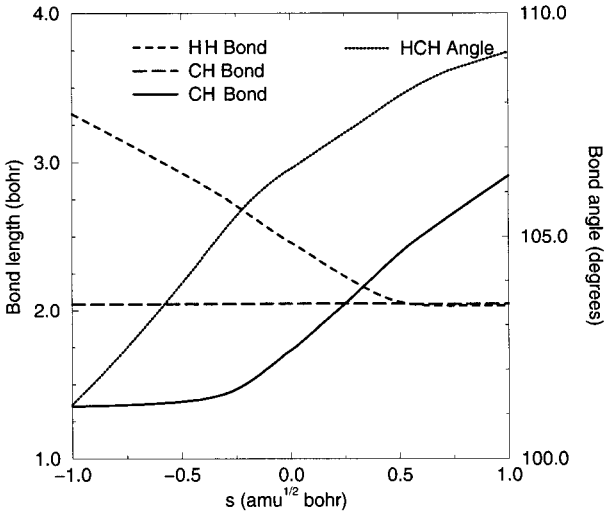

FIGURE 1. Plots of geometrical parameters of the $H_2 + CH_3 \rightarrow H + CH_4$ reaction versus the reaction coordinate. The dotted curve represents the HCH bond angle (degrees). Various bond lengths (bohr) are also shown.

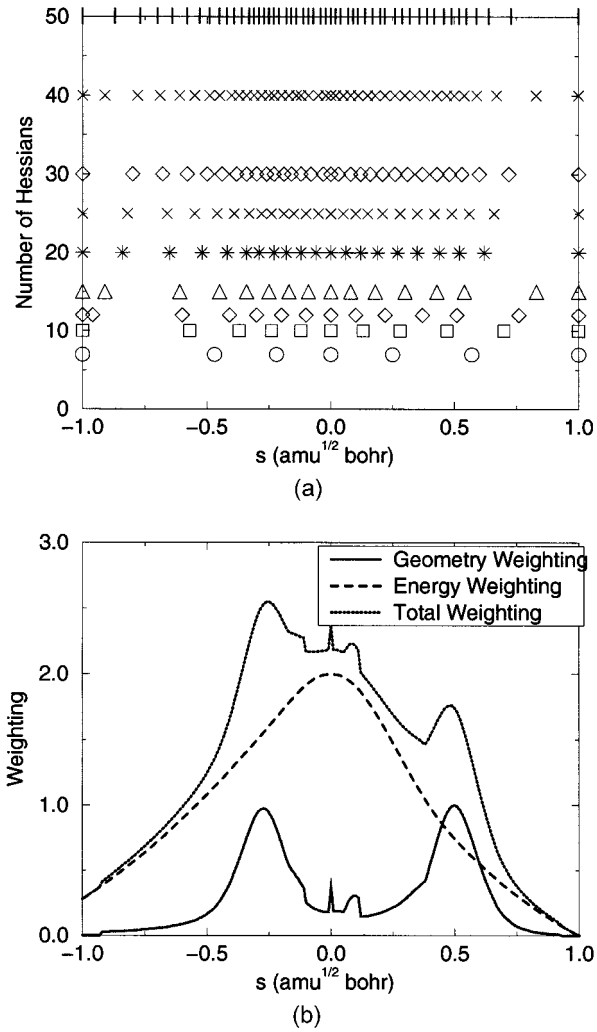

FIGURE 2. (a) Plot of locations of the Hessian grids selected by the focusing technique for each given number of Hessian points. (b) Plot of the weighting curves. The normalized potential energy, the normalized sum of the geometrical second derivative components, and the total weighting are shown.

Note the locations of the two peaks (-0.30 and -0.45 amu$^{1/2}$bohr) in the second derivative of the geometries (see Fig. 1) coincide with the peaks of the B_{mf} coupling.

Figures 5 and 6 show the convergence of CVT rates as a function of the number of Hessian calculations. This reaction involves transfer of the light hydrogen atom, so tunneling plays a significant role. The CVT rate constants have converged to a final result with only seven Hessian grid points. Likewise, the CVT rate constant with the zero-curvature tunneling correction also converges with only seven Hessian grid points. SCT tunneling,

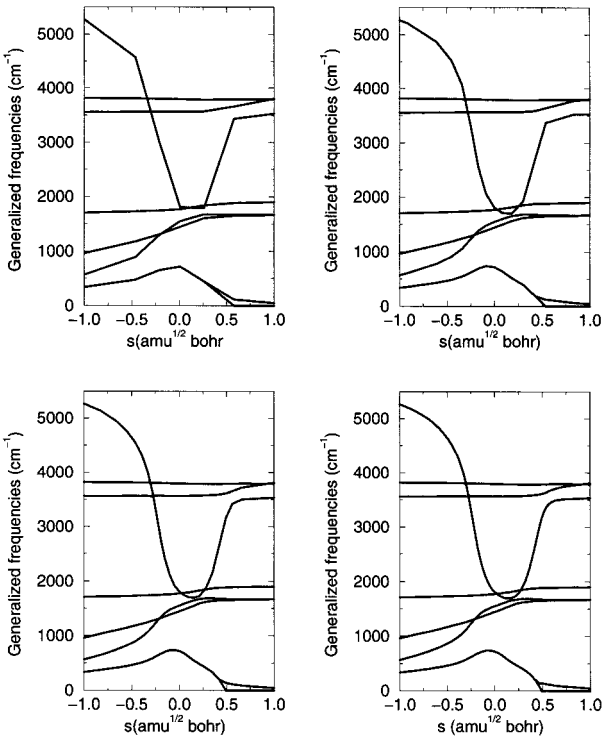

FIGURE 3. Generalized frequencies of the $H_2 + CH_3$ reaction plotted versus reaction coordinate. The Hessian grid for each graph is: upper left — 7; upper right — 15; lower left — 25; lower right — 50.

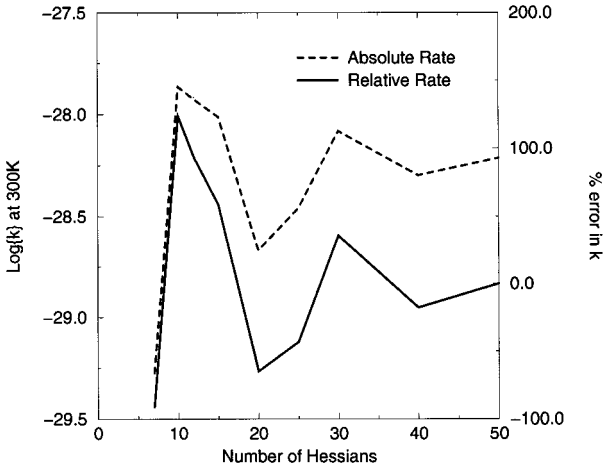

FIGURE 5. Convergence of the CVT / SCT rate constant at 300 K with respect to the number of Hessian grid points. The solid line gives the percent difference from the 50-Hessian rate. The dashed line is a log plot of the actual rate constants.

however, requires at least 30 Hessian calculations to converge to within 40%. An important implication of this is that if the CVT dividing surface remains close to the transition state, and if tunneling is not important, accurate results may be obtained with fewer Hessian calculations. As tunneling becomes more important, more Hessian points

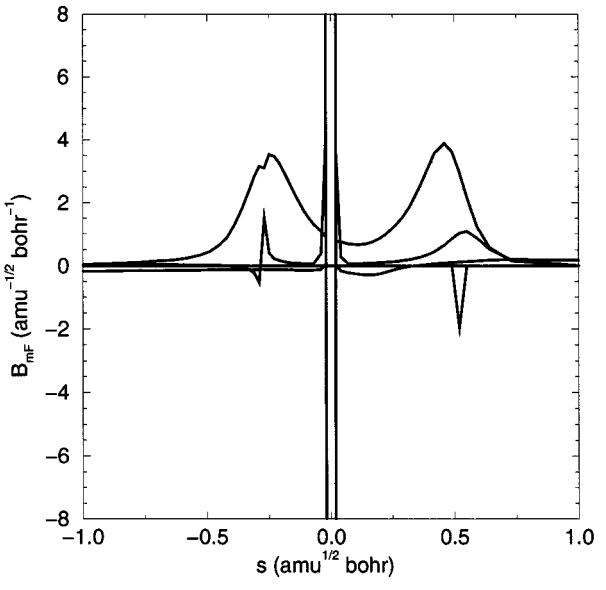

FIGURE 4. B_{mf} coupling of the $H_2 + CH_3$ reaction plotted versus reaction coordinate.

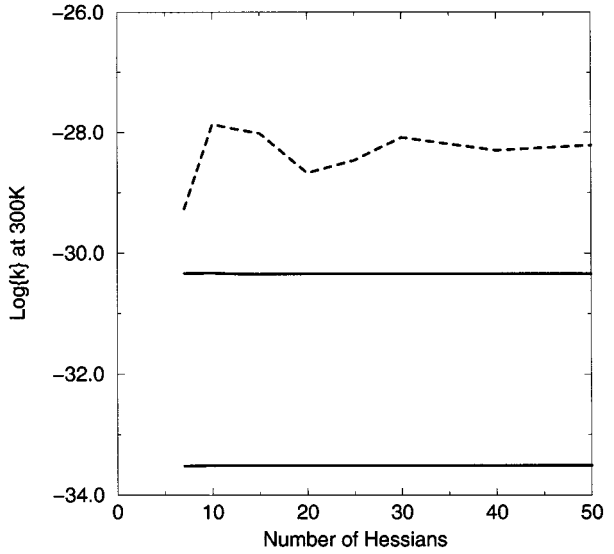

FIGURE 6. Similar to Figure 5 except for different levels of theory. The lower curve is the CVT rate. The middle curve is the CVT / ZCT rate. The upper dashed curve is the CVT / SCT rate.

are needed to model the reaction path curvature accurately.

ANALYSIS OF ENERGY INTERPOLATION PROCEDURE

We have performed single-point energy calculations using MP2 (Møller–Plesset perturbation theory) with the 6-31G basis set. Figure 7 shows a comparison of the UHF/STO-3G and MP2/6-31G//UHF/STO-3G potential curves, whereas Figure 8 shows convergence of the MP2 energies with increasing number of energy calculations. The relative inaccuracy of the HF theory and STO-3G basis set used in the low-level calculations gives our energy interpolation scheme a severe test. The Hartree–Fock geometries are quite different from the geometry results of the more accurate MP2 calculation. In a practical sense, this means that the potential energy peak is shifted noticeably as energy corrections are added. Even for this severe case scenario, only 11 (one third of Hessian points) additional energy calculations plus the stationary points are required to converge the rate calculation. Figure 9 shows the rate convergence as the number of energy replacement points increase. Systems which use a better theoretical method for calculating the MEP will require fewer energy replacement points.

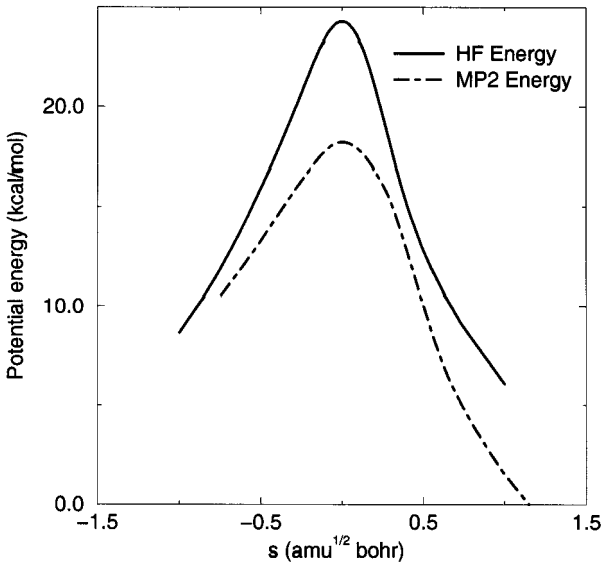

FIGURE 7. HF and MP2 // HF potential energies along the reaction coordinate. The MP2 // HF energies were obtained at every Hessian grid point. Both plots use the 30-point Hessian grid.

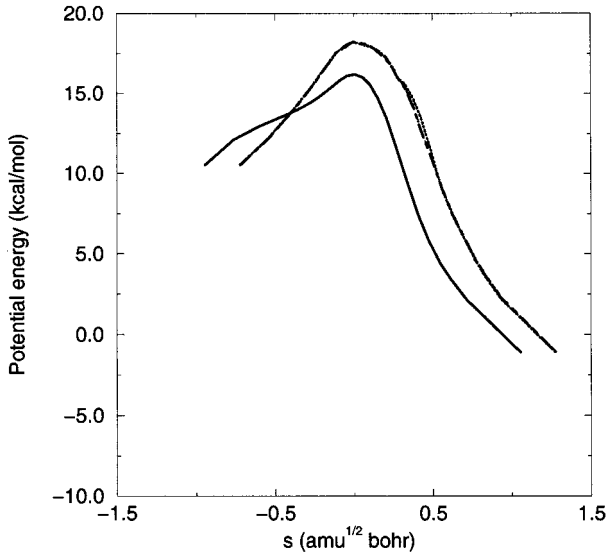

FIGURE 8. MP2 // HF potential energy curves interpolated from a different number of single-point energy calculations. The solid line represents an energy interpolation from 7 single-point energies, the dotted line from 11 points, and the dashed line from 15 points.

Conclusion

Computational and theoretical advances have progressed sufficiently so that it is now possible to calculate reaction rates directly from *ab initio* the-

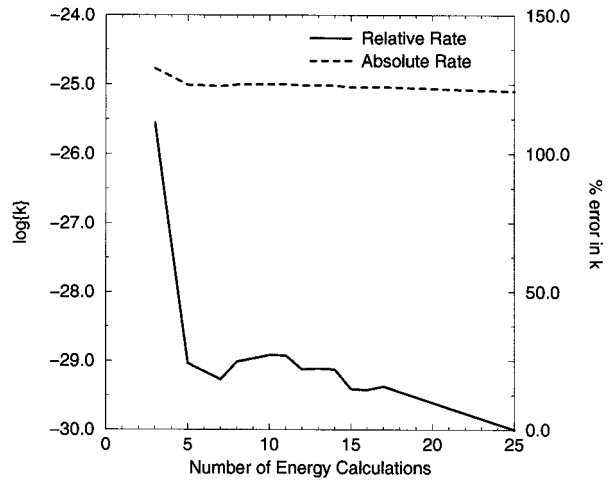

FIGURE 9. Convergence of the CVT / SCT rate constant at 300 K with respect to the number of single-point energies. The solid line gives the percent difference from the 30-point rate. The dashed line is a log plot of the actual rate constant.

ory without the intervening use of an analytical potential energy surface. We have developed the TheRate (Theoretical Rates) program to perform such calculations efficiently. The number of calculations required for a variational transition-state calculation with semiclassical tunneling calculations is gratifyingly small—fewer than would normally be required in constructing a high-quality analytical potential energy surface. An intelligent choice of points at which to calculate the frequencies should require fewer than 30 Hessian calculations for the typical system. Improvement of the energetics requires still fewer *ab initio* calculations, which is convenient as these often require robust levels of theory to obtain accurate theoretical rates.

We have used the $CH_4 + H \leftrightarrow CH_3 + H_2$ reaction to examine our Hessian focusing routine and energy replacement technique. These results provide a baseline for the number of Hessian calculations and single-point energy calculations that are required.

Finally, TheRate provides a user-friendly environment making it a promising computational tool for both teaching and research. For further information on obtaining TheRate, please see our web page at http://www.usi.utah.edu/research/TheRate.

Appendix A

TECHNICAL CONSIDERATIONS

Vibrational mode correlation. A new vibrational mode correlation routine is utilized here. The traditional way for correlating modes uses mode–mode overlap between adjacent points on the MEP.[23] For the most part, this procedure is very successful for small systems. For larger systems, in which multiple mode crossings may occur within a small interval of the reaction coordinate, this overlap criterion is not always sufficient to discriminate between modes. This problem is responsible for the apparent avoided crossings between modes in plots of generalized frequencies versus reaction coordinate.

The new routine solves this problem by calculating additional overlap matrices not only between adjacent points but also between points up to two reaction coordinate positions apart. If the adjacent overlap fails to achieve minimum correlation levels, the routine attempts to correlate either forward or backward up to a maximum of two reaction coordinate positions to make a better choice.

Focusing technique. This range of data points defaults to 8 and may be changed by the user. As mentioned earlier, the first few steps along the MEP from the transition state are somewhat erratic. Thus we interpolate data points in the transition-state region rather than use the raw data. The number of data points to be interpolated may be changed by the user. The default value is 2.

MEP Calculations. As the MEP approaches the reactant and product regions, the gradient becomes small. This directly affects the stability of the numerical techniques used to find the MEP, and as a result small oscillations in the geometrical parameters often occur. The numerically calculated derivatives in the tunneling calculations are especially susceptible to these errors. However, it is not necessary to integrate the MEP far into these regions for rate calculations.

The range of the MEP needed for rate calculations varies depending on the type of reaction. For typical reactions involving transfer of a light particle, tunneling is often quite significant and larger MEP ranges are needed to ensure inclusion of regions having large curvature. However, for reactions where tunneling is anticipated to be small, smaller ranges of MEP values are sufficient. With the use of the extrapolation to the reactant and product limits described next, the MEP range including the top half of the barrier is normally sufficient.

Extrapolations to reactants and products. Calculation of the $\theta(E)$ integral requires knowing the classical turning points, s_r, and s_l, at the energy, E. As discussed in the previous subsection, it is not necessary to integrate far into the reactant and product channels. However, to converge the tunneling probability, the MEP is extrapolated to the reactant and product stationary states using an exponential form given by:

$$E = V(1 + \alpha e^{\gamma s}) \tag{32}$$

where V is the energy at the reactant (or product) and the variables γ and α are adjusted so the curve and its first derivative are continuous at the connecting point.

Smoothing the μ_{eff}. Small oscillations in the numerically produced MEP may lead to noise in the calculated reaction path curvature and, subsequently, in μ_{eff} [eq. (20)]. We compensate for this effect by removing high-frequency oscillations in

the μ_{eff} data. This is done using a fast Fourier transform low-pass filter. The endpoints are assigned the value of μ before the Fourier transform to resolve problems with the one-sided numerical derivatives at these points.

Integration. Numerical integrations are performed using a globally adaptive Gaussian–Konrad quadrature scheme.[80] This same approach is used for integration of both of eqs. (12) and (14). The globally adaptive procedure starts with a 21-point Konrad quadrature integration and, if the estimated error is too large, progressively subdivides the intervals until the estimated error converges below an acceptable precision of (1.0E-3).

Appendix B

PROGRAM USAGE AND CONSIDERATIONS

Supported platforms and availability. TheRate is Java based and runs on any platform with JDK 1.1.5, or better, which is freely available on most Unix platforms, as well as Macintosh and PC compatibles. A network connection is required.

Associated software. TheRate is currently configured to use Gaussian-94 as the basis for all electronic structure calculations. Interfacing TheRate with other electronic structure packages is easily done by rewriting the parsing classes. If interested, please contact: Truong@chemistry.utah.edu

References

1. J. Warnatz, In *Combustion Chemistry*, W. C. J. Gardiner, Ed., Springer, New York, 1984, p. 233.
2. D. J. Hucknall, *Chemistry of Hydrocarbons*, Chapman and Hall, London, 1985.
3. F. S. Rowland and M. J. Molina, *Reviews of Geophysics and Space Physics*, **13**, 1 (1975).
4. I. W. M. Smith, *Kinetics and Dynamics of Elementary Gas Reactions*, Butterworths, Boston, 1980.
5. D. H. Zhang and J. Z. H. Zhang, *J. Chem. Phys.*, **101**, 1146 (1994).
6. J. Echave and D. C. Clary, *J. Chem. Phys.*, **100**, 402 (1994).
7. D. Neuhauser, *J. Chem. Phys.*, **100**, 9272 (1994).
8. U. Manthe, T. Seideman, and W. H. Miller, *J. Chem. Phys.*, **99**, 10078 (1993).
9. H. Szichman, I. Last, A. Baram, and M. Baer, *J. Phys. Chem.*, **97**, 6436 (1993).
10. W. L. Hase, *J. Chem. Phys.*, **64**, 2442 (1976).
11. M. Quack and J. Troe, *Ber. Bunsenges. Phys. Chem.*, **81**, 329 (1977).
12. D. G. Truhlar, Ed., *Potential Energy Surfaces and Dynamics Calculations*, Plenum Press, New York, 1981.
13. T. Joseph, R. Steckler, and D. G. Truhlar, *J. Chem. Phys.*, **87**, 7036 (1987).
14. R. Steckler, F. B. Brown, K. J. Dykema, G. C. Hancock, D. G. Truhlar, and T. Valencich, *J. Chem. Phys.*, **87**, 7024 (1987).
15. D. G. Truhlar, M. S. Gordon, and R. Steckler, *Chem. Rev.*, **87**, 217 (1987).
16. J. C. Corchado, J. Espinosa-Garcia, W.-R Hu, I. Rossi, and D. G. Truhlar, *J. Phys. Chem.*, **99**, 687 (1995).
17. T. N. Truong, *J. Chem. Phys.*, **100**, 8014 (1994).
18. T. N. Truong and W. Duncan, *J. Phys. Chem.*, **101**, 7408 (1994).
19. D. G. Truhlar, In *The Reaction Path in Chemistry: Current Approaches and Perspectives*, P. Heidrich, Ed., Kluwer, Dordrecht, 1995, p. 229.
20. I. S. Y. Wang and M. Karplus, *J. Am. Chem. Soc.*, **95**, 8160 (1973).
21. C. Leforestier, *J. Chem. Phys.*, **68**, 4406 (1978).
22. W. H. Miller, N. C. Handy, and J. E. Adams, *J. Chem. Phys.*, **72**, 99 (1980).
23. D. G. Truhlar, A. D. Isaacson, and B. C. Garrett, In *Theory of Chemical Reaction Dynamics*, M. Baer, Ed., CRC Press, Boca Raton, FL, 1985, p. 65.
24. K. K. Baldridge, M. S. Gordon, R. Steckler, and D. G. Truhlar, *J. Phys. Chem.*, **93**, 5107 (1989).
25. G. D. Billing, *Chem. Phys.*, **89**, 199 (1984).
26. K. Fukui, *Acc. Chem. Res.*, **14**, 363 (1981).
27. D. G. Truhlar, B. C. Garrett, and S. J. Klippenstein, *J. Phys. Chem.*, **100**, 12771 (1996).
28. S. C. Tucker and D. G. Truhlar, In *Dynamical Formulation of Transition State Theory: Variational Transition States and Semiclassical Tunneling*, J. Bertran and I. G. Csizmadia, Eds., Advanced Study Institute, Kluwer, Dordrecht, 1989, p. 291.
29. A. Gonzalez-Lafont, T. N. Truong, and D. G. Truhler, *J. Chem. Phys.*, **95**, 8875 (1991).
30. A. Gonzalez-Lafont, T. N. Truong, and D. G. Truhlar, *J. Phys. Chem.*, **95**, 4618 (1991).
31. I. Rossi and D. G. Truhlar, *Chem. Phys. Lett.*, **233**, 231 (1995).
32. M. J. Field, *Chem. Phys. Lett.*, **172**, 83 (1990).
33. B. C. Garrett, M. L. Koszykowski, C. F. Melius, and M. Page, *J. Phys. Chem.*, **94**, 7096 (1990).
34. T. N. Truong and D. G. Truhlar, *J. Chem. Phys.*, **93**, 1761 (1990).
35. B. C. Garrett and C. F. Melius, In *Theoretical and Computation Models for Organic Chemistry*, S. J. Formosinho, I. G. Dxizmadia, and L. G. Arnaut, Eds., Kluwer, Dordrecht, 1991, p. 25.
36. Y.-P Liu,, D.-H. Lu, A. Gonzalez-Lafont, D. G. Truhlar, and B. C. Garrett, *J. Am. Chem. Soc.*, **115**, 7806 (1993).
37. R. L. Bell and T. N. Truong, *J. Chem. Phys.*, **101**, 10442 (1994).
38. Q. Zhang, R. Bell, and T. N. Truong, *J. Phys. Chem.*, **99**, 592 (1995).
39. E. Kraka, J. Gauss, and D. Cremer, *J. Chem. Phys.*, **99**, 5306 (1993).

40. V. S. Melissas and D. G. Truhlar, *J. Chem. Phys.*, **99**, 1013 (1993).
41. V. S. Melissas and D. G. Truhlar, *J. Phys. Chem.*, **98**, 875 (1994).
42. R. Steckler, W. P. Hu, Y. P. Liu, G. C. Lynch, B. C. Garrett, A. D. Isaacson, V. S. Melissas, D. H. Lu, T. N. Truong, N. R. Sachchida, G. C. Hancock, J. G. Lauderdale, T. Joseph, and D. G. Truhlar, *Comput. Phys. Commun.*, **88**, 341 (1995).
43. H. H. Bueker, T. Helgaker, K. Ruud, and E. Uggerud, *J. Phys. Chem.*, **100**, 15388 (1996).
44. C. Doubleday, K Bolton, G. H. Peslherbe, and W. L. Hase, *J. Am. Chem. Soc.*, **118**, 9922 (1996).
45. G. M. Peslherbe and W. L. Hase, *J. Chem. Phys.*, **104**, 7882 (1996).
46. K. A. Nguyen, I. Rossi, and D. G. Truhlar, *J. Chem. Phys.*, **103**, 5522 (1995).
47. W. T. Duncan and T. N. Truong, *J. Chem. Phys.*, **103**, 9642 (1995).
48. T. N. Truong and T. J. Evans, *J. Phys. Chem.*, **98**, 9558 (1994).
49. T. N. Truong, *J. Chem. Phys.*, **102**, 5335 (1995).
50. R. L. Bell, D. L. Taveras, T. N. Truong, and J. Simons, *Int. J. Quantum Chem.*, **63**, 861 (1997).
51. R. L. Bell and T. N. Truong, *J. Phys. Chem. A*, **101**, 7802 (1997).
52. A. D. Becke, *J. Chem. Phys.*, **84**, 4524 (1986).
53. A. D. Becke, *J. Chem. Phys.*, **98**, 1372 (1993).
54. C. Lee, W. Yang, and R. G. Parr, *Phys. Rev. B*, **37**, 785 (1988).
55. M. J. Frisch, G. W. Trucks, H. B. Schlegel, P. M. W. Gill, B. G. Johnson, M. A. Robb, J. R. Cheeseman, T. Keith, G. A. Petersson, J. A. Montgomery, K. Raghavachari, M. A. Al-Laham, V. G. Zakrzewski, J. V. Ortiz, J. B. Foresman, J. Cioslowski, B. B. Stefanov, A. Nanayakkara, M. Challacombe, C. Y. Peng, P. Y. Ayala, W. Chen, M. W. Wong, J. L. Andres, E. S. Replogle, R. Gomperts, R. L. Martin, D. J. Fox, J. S. Binkley, D. J. Defrees, J. Baker, J. P. Stewart, M. Head-Gordon, C. Gonzalez, and J. A. Pople, *Gaussian-94* (*Revision B.*), Gaussian, Inc., Pittsburgh, PA, (1995).
56. T. N. Truong, W. T. Duncan, and R. L. Bell, In *Chemical Applications of Density-Functional Theory*, B. B. Laird, R. B. Ross, and T. Ziegler, Eds., American Chemical Society, Washington, DC, 1996, p. 85.
57. J. S. Winn, *Physical Chemistry*, HarperCollins, New York, 1995.
58. P. W. Atkins, *Physical Chemistry, 4th Ed.*, W. H. Freeman & Co., New York, 1990.
59. G. D. Billing and K. V. Mikkelsen, *Introduction to Molecular Dynamics and Chemical Kinetics*, John Wiley & Sons, New York, 1996.
60. H. S. Johnston, *Gas Phase Reaction Rate Theory*, Ronald Press, New York, 1966.
61. S. Glasstone, K. J. Laidler, and H. Eyring, *Theory of Rate Processes*, McGraw-Hill, New York, 1941.
62. P. Pechukas, In *Dynamics of Molecular Collisions—Part B*, W. H. Miller, Ed., Plenum Press, New York, 1976, p. 269.
63. D. A. McQuarrie, *Statistical Mechanics*, HarperCollins, New York, 1976.
64. E. Wigner, *J. Chem. Phys.*, **5**, 720 (1937).
65. J. Horiuti, *J. Bull. Chem. Soc. Jpn.*, **13**, 210 (1938).
66. J. Keck, *Adv. Chem. Phys.*, **13**, 85 (1967).
67. D. G. Truhlar and B. C. Garrett, *Annu. Rev. Phys. Chem.*, **35**, 159 (1984).
68. T. Baer and W. L. Hase, *Unimolecular Reaction Dynamics (International Series of Monographs on Chemistry)*, Oxford University Press, New York, 1996.
69. K. J. Laidler, *Chemical Kinetics* (*3rd Ed.*) Harper & Row, New York, 1987.
70. R. G. Gilbert and S. C. Smith, *Theory of Unimolecular and Recombination Reactions*, Blackwell, Oxford, 1990.
71. A. Vincent, *Molecular Symmetry and Group Theory*, John Wiley & Sons, New York, 1977.
72. Y.-P Liu, G. C. Lynch, T. N. Truong, D.-H. Lu, D. G. Trublar, and B. C. Gerrett, *J. Am. Chem. Soc.*, **115**, 2408 (1993).
73. D. H. Lu, T. N. Truong, V. S. Melissas, G. C. Lynch, Y. P. Liu, B. C. Garrett, R. Steckler, A. D. Isaacson, S. N. Rai, G. C. Hancock, J. G. Lauderdale, T. Joseph, and D. G. Truhlar, *Comput. Phys. Comm.*, **71**, 235 (1992).
74. R. A. Marcus and M. E. Coltrin, *J. Chem. Phys.*, **67**, 2609 (1977).
75. M. Page and J. W. McIver Jr., *J. Chem. Phys.*, **88**, 922 (1988).
76. D. G. Truhlar and A. D. Isaacson, *J. Chem. Phys.*, **77**, 3516 (1982).
77. M. Quack and J. Troe, *Ber. Bunsenges. Phys. Chem.*, **78**, 240 (1974).
78. C. Gonzalez and H. B. Schlegel, *J. Chem. Phys.*, **90**, 2164 (1989).
79. C. Gonzalez and H. B. Schlegel, *J. Phys. Chem.*, **94**, 5523 (1990).
80. R. Piessens, E. deDoncker Kapenga, C. Uberhuber, and D. Kahaner, In *Series in Computational Mathematics*, Vol. 1, Springer, Berlin, 1983.